Acta Astronautica ▮ (▮▮▮▮) ▮▮▮–▮▮▮

Contents lists available at ScienceDirect

Acta Astronautica

journal homepage: www.elsevier.com/locate/actaastro

Two models of force actuator based active suspension mechanisms for mobility on uneven terrain

Vijay P. Eathakota *, Arun K. Singh, K. Madhava Krishna

Robotics Research Center, International Institute of Information Technology, Hyderabad, India

ARTICLE INFO

Article history:
Received 15 October 2009
Received in revised form
28 May 2010
Accepted 26 June 2010

Keywords:
Force control
Active suspension vehicles
Linear force actuator
Legged robots
Wheeled robots
Uneven terrain navigation

ABSTRACT

In this paper we present two mechanisms of linear force actuator based actively articulated suspension vehicles and propose a strategy to control the wheel–ground contact forces to improve traction and to increase the no-slip margin and hence enhance the mobility of the vehicle on uneven terrain. We present the quasi-static analysis of each of the mechanisms to depict the ability of the systems to control the wheel–ground contact forces while negotiating uneven terrain with the help of feasibility plots. The first model is a vehicle with a 1-*dof* leg (referred to as LFA-V1) and can climb slopes upto 40 degrees but to further increase the capability of the robot we come with a modified design of the vehicle which has a 2-*dof* leg (referred to as LFA-V2) and can negotiate slopes with discontinuities greater than twice the wheel diameter.

1. Introduction

To improve the mobility of wheeled robots traversing on a fully 3D uneven terrain while maintaining a stable posture is the primary focus of our research. Most of the research in this field was encouraged by the idea of finding suspension mechanisms suitable for space exploration. This finds special application in space exploration where the normal forces are reduced because of the reduction in the gravitational force resulting in the reduction in the limit of the maximum torque that can be generated without incurring slip. Past research on 'all terrain vehicles' [1,2] was focused on developing mechanical suspension systems, which could improve terrain adaptability and locomotion. Shrimp robots [1] and Rocky rovers [2] are terrain vehicles with passive suspension systems, which have excellent terrain adaptability and ability to negotiate terrains having discontinuities that are higher than the wheel radius. However, such systems do not have the ability to control the contact forces at the wheel–ground contact points. Hence, Sreenivasan and Waldron [4] developed vehicles called Wheeled and Actively Articulated Vehicles (WAAVs). These vehicles are distinct from traditional wheeled systems since they have the ability to actively adapt to variations in the terrain and they can actively influence the forces at the wheel–terrain contact locations. Grand et al [5,8], developed an actively articulated suspension vehicle called Hylos. Posture control algorithm for Hylos was developed by mapping the velocities at various joints to the velocity of the main body based on posture error, which improves traction and stability. Iagnemma et al. [3] and Iagnemma and Dubowsky [6] developed a traction control algorithm to improve ground traction of a vehicle traversing on rough terrain while optimizing power consumption. The above methods achieved rough terrain navigation essentially by a posture adaptation framework. By changing the posture according to the underlying terrain the above methods redistributed the normal forces acting on the vehicle to negotiate uneven and undulating terrain.

In our work we go beyond redistribution of normal forces and create additional contact forces to allow for enhanced traction as well as to increase the no-slip margin. This is

* Corresponding author.
E-mail addresses: eathakota.vijay@iiit.ac.in (V.P. Eathakota), aks1812@gmail.com (A.K. Singh), mkrishna@iiit.ac.in (K. Madhava Krishna).

0094-5765/$ - see front matter © 2010 Elsevier Ltd. All rights reserved.
doi:10.1016/j.actaastro.2010.06.051

realized through a linear force actuator based vehicle (LFA-V) that achieves required traction by directly controlling the contact forces at the wheels of the vehicle. We model the wheels as a torus to simulate a single point contact with the terrain [13]. The idea of generating additional forces follows from the D'Alembert's principle of inertial forces and we explain the idea in more detail in the following sections. In this paper we propose two models of linear force actuator based suspension vehicles (LFA-Vs) having 1-*dof* and 2-*dof* actuated prismatic legs. We depict the force controllability of these mechanisms by computing feasibility regions. For brevity of analysis, we will refer to the LFA-V with 1-*dof* actuated prismatic leg as LFA-V1 and the other as LFA-V2.We have also introduced a framework for calculating the traction forces from the sensor readings at the contact points of each wheel and present the quasi-static analysis of our suspension mechanisms in a general 3D reference frame, which follows from the fixed suspension model and the planar LFA-V model developed in our earlier work in [10], and the 3D model of the LFA-V developed by us in [15]. Another mechanism, which uses linear actuators as a suspension mechanism is the BOSE suspension [11], which uses a linear actuator to sense bumps and undulations on the road and command the desired actuator length to keep the posture/car level. But since it is applied for a fast moving vehicle, implementation of traction optimization is not present and the size of undulations traversed it is much smaller than the wheel diameter.

Whereas the mechanisms proposed in our work the linear actuators provide for both traction and posture control and the vehicle negotiates terrain discontinuities or steps, which are more than the wheel diameter. Moreover, the BOSE suspension mechanism in [11] does not modify posture of the vehicle in a force actuated manner to change the wheel–ground contact forces. In our work we exploit the internal mobility of the mechanism to control the wheel–ground contact forces.

The novelties of the paper include the two new force actuator based mechanisms for rough terrain navigation, the development of a completely 3D framework for control and analysis of both these mechanisms and the depiction of feasibility plots showing the traversability in uneven terrain of the 1-*dof* leg based design and the 2-*dof* leg based design. The regions of traversal as predicted by the analysis of the quasi-static framework are verified in extensive simulations on a dynamic simulation engine (MSC–VisualNastran).

2. Quasi-static analysis of LFA-V1

In this section the mechanical model of the LFA-V having a 1-*dof* actuated leg is developed and the force control strategy at the wheel–ground contact point is explained. Fig. 1 shows the mechanical structure consisting of 4 wheels each pinned to an outer slide link, which is connected to an inner slide link through a prismatic joint. The inner slide is fixed to the chassis. To achieve a desired value of the contact force at the *i*th wheel force control mechanism is proposed in which the prismatic joint is actuated through a linear actuator

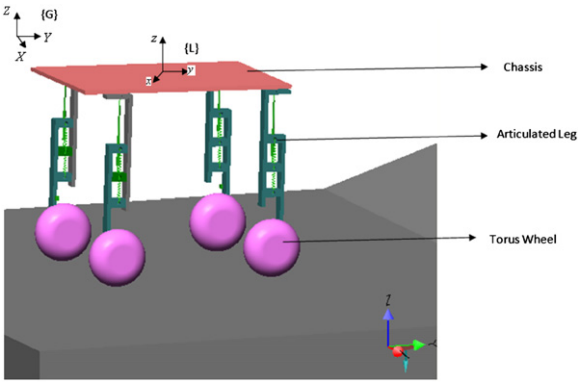

Fig. 1. The LFA-V1 mechanical structure.

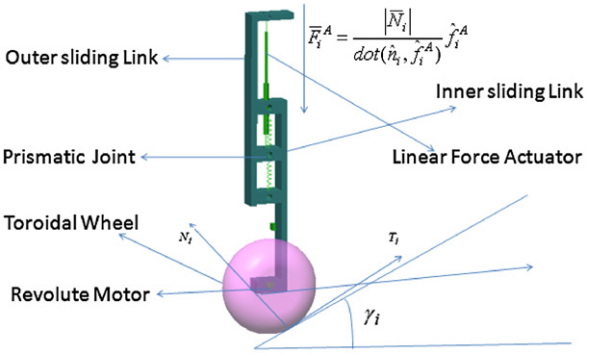

Fig. 2. The LFA-V1 actuated leg.

mounted on the chassis to which a required force $\vec{F}_i^A$ can be commanded. This force acts between the main body and the output slide. Although the input and output slides have finite mass, they are considered to be negligible when compared to the mass of the chassis and hence neglected in the analysis.

Force control of the LFA-V is achieved based on D'Alembert's principle of inertial forces. As shown in Figs. 2 and 3 the actuator force acting through the prismatic joint causes a force on the chassis and accelerates it upwards. The accelerating chassis can be converted to an equivalent static chassis by adding a pseudo-force in the downward direction and this in turn increases the reaction normal forces.

Next the quasi-static force balance equations are developed for this model. Fig. 4a shows the description of LFA-V1 as a parallel manipulator where $P_i \forall i=\{1,2,3,4\}$ are prismatic joints and $R_i \forall i=\{1,2,3,4\}$ are revolute joints and the wheel–ground contact point is modeled as an instantaneous 3-*dof* non-holonomic joint. The total number of degrees of internal mobility of this parallel manipulator can be calculated using Grubler's equation for spatial manipulators given by

$$dof = 6(N-J-1)+\sum_{i=1}^{J} F_i \tag{1}$$

where N is the total number for bodies, J the total number of joints and F_i the degree of freedom for each joint. For

Please cite this article as: V.P. Eathakota, et al., Two models of force actuator based active suspension mechanisms for mobility on uneven terrain, Acta Astronautica (2010), doi:10.1016/j.actaastro.2010.06.051

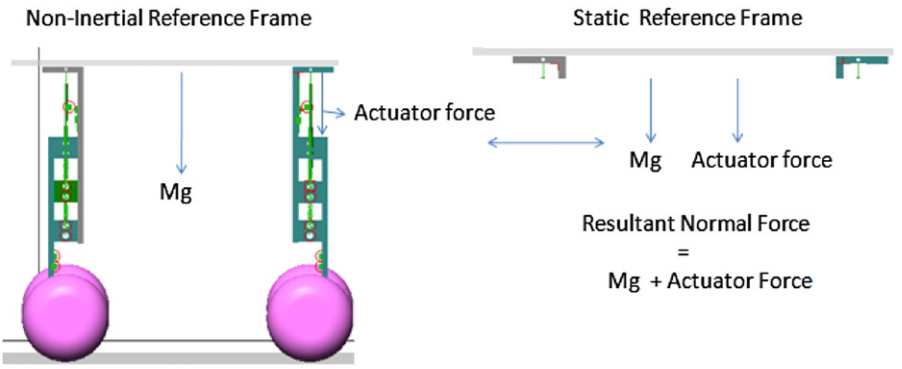

Fig. 3. D'Alembert's principle of inertial forces.

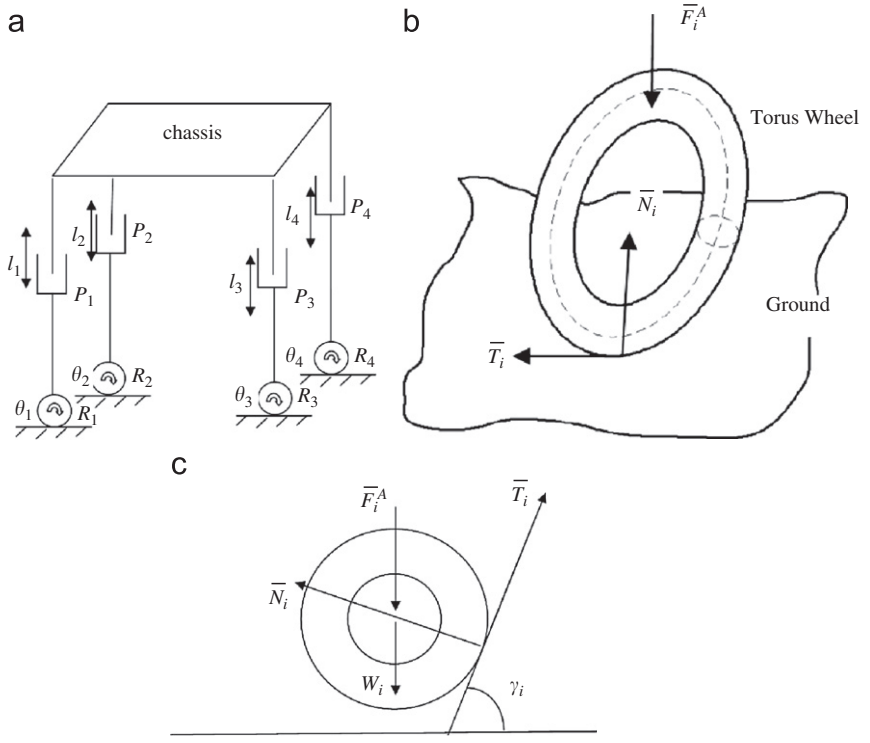

Fig. 4. (a) LFA-V1 as a parallel manipulator. (b) A Torus shaped wheel on uneven terrain. (c) Free body diagram of the wheel.

the parallel manipulator of Fig. 4 we have N equals to 14 (three bodies for each leg, which include wheel and 2 parts of the prismatic joint and the platform and the ground), J equals to 16 (3 joints in each leg and 4 wheel–ground contact points) and $\sum_{i=1}^{J} F_i$ equals to 20 (1-*dof* rotational and prismatic joint for each leg and an instantaneous 3-*dof* joints at each wheel–ground contact point with ideal rolling constraint and the joint between the prismatic pair and the chassis is rigid with 0 *dof*) and hence overall *dof* of the system can be found to be 2.

The LFA-V1 is a redundantly actuated vehicle with 8 actuated joints including the wheels. To develop the quasi-static force balance equation for the LFA-V1 a method of estimating the traction forces from the sensor readings of the contact forces is developed. Then, the net force and moments acting on the chassis of the vehicle are determined assuming the vehicle to be an ideal suspension. The mass of the legs is assumed to be negligible when compared to the mass of the chassis. Finally, the control laws for force and moment control to retain a stable posture of the vehicle during navigation are derived.

2.1. Estimating the traction forces from sensor readings

Let ψ, α and β be the pitch, roll and yaw angles, respectively, of the chassis about the global $\{G\}$ axes. The local and global frames ($\{L\}$,$\{G\}$) are shown in Fig. 1. The resultant rotation matrix relating position vectors and the force components at various points to the reference

Please cite this article as: V.P. Eathakota, et al., Two models of force actuator based active suspension mechanisms for mobility on uneven terrain, Acta Astronautica (2010), doi:10.1016/j.actaastro.2010.06.051

frame of the chassis is

$$R = R_z(\beta)R_y(\alpha)R_x(\psi) \tag{2}$$

where $R_x(\psi)$, $R_y(\alpha)$ and $R_z(\beta)$are the rotation matrices corresponding to the Euler angles about the X, Y and Z axes, respectively. From Fig. 4b the forces acting at the ith wheel of the vehicle from the chassis (local frame {L}) reference frame are

i) The normal force $\vec{N}_{iL} = \begin{bmatrix} N_{xi} & N_{yi} & N_{zi} \end{bmatrix}^T$

ii) The traction force $\vec{T}_{iL} = \begin{bmatrix} T_{xi} & T_{yi} & T_{zi} \end{bmatrix}^T$

iii) The actuator force $\vec{F}^A_i$, which is always perpendicular to the chassis.

The normal forces and the Euler angles are assumed to be obtained from the sensor readings. The normal forces can be sensed when the robot is equipped with tactile wheels. Tactile wheels [14] give approximate information about the value of the normal contact force and its direction. The Euler angles, which give information of the posture of the chassis can be measured using an inertial measurement unit (IMU). The motion of the vehicle is assumed to be non-holonomic in nature, which means that the vehicle's velocity along the lateral direction is negligible and hence from the chassis reference frame

$$T_{xi} \approx 0 \text{ and } T_{yi} > 0. \tag{3}$$

Under no-slip conditions

$$|\vec{T}_{iL}| \le \mu_i |\vec{N}_{iL}| \forall i = \{1,2,3,4\} \tag{4}$$

where μ_i is the coefficient of friction between the point of contact of ith wheel and the terrain.

Since $\vec{T}_{iL}$ is always perpendicular to $\vec{N}_{iL}$

$$\vec{N}_{iL} \cdot \vec{T}_{iL} \Rightarrow N_{xi}T_{xi} + N_{yi}T_{yi} + N_{zi}T_{zi} = 0 \tag{5}$$

From (3)

$$|\vec{T}_{iL}| = \eta_i\mu_i|\vec{N}_{iL}| \Rightarrow T_{xi}^2 + T_{yi}^2 + T_{zi}^2 = (\eta_i\mu_i)^2 N_{iL}^2 \tag{6}$$

where $0 < \eta_i \le 1 \forall i = \{1,2,3,4\}$

If $|\vec{N}_{iL}| \neq 0$ then any one of the components N_{xi}, N_{yi}, $N_{zi} \neq 0$, in general $N_{zi} \neq 0$, as long as the wheels remain in contact, then from (5) and (6) we get

$$(\eta_i\mu_i)^2 |\vec{N}_{iL}|^2 - T_{xi}^2 = T_{yi}^2 + \left[\frac{N_{xi}T_{xi} + N_{yi}T_{yi}}{N_{zi}}\right]^2 \tag{7}$$

Simplifying the above we get in the form

$$aT_{yi}^2 + bT_{yi} + c = 0 \tag{8}$$

Solving the above quadratic equation we get

$$T_{xi} = \frac{\eta_i\mu_i|\vec{N}_{iL}||N_{zi}|}{\sqrt{N_{zi}^2 + N_{yi}^2}} \text{ and } T_{zi} = \frac{-\eta_i\mu_i N_{yi}|\vec{N}_{iL}||N_{zi}|}{N_{zi}\sqrt{N_{zi}^2 + N_{yi}^2}} \tag{9}$$

Now the unit vectors of $\vec{T}_{iL}$ and $\vec{N}_{iL}$ in the global reference frame are

$$\hat{t}_i = R\frac{\vec{T}_{iL}}{|\vec{T}_{iL}|} = \begin{bmatrix} t_{Xi} & t_{Yi} & t_{Zi} \end{bmatrix}^T \text{ and } \hat{n}_i = R\frac{\vec{N}_{iL}}{|\vec{N}_{iL}|} = \begin{bmatrix} n_{Xi} & n_{Yi} & n_{Zi} \end{bmatrix}^T \tag{9.a}$$

$$\vec{T}_i = R\vec{T}_{iL} \text{ and } \vec{N}_i = R\vec{N}_{iL} \tag{9.b}$$

are the traction and normal forces at the point contact in the global reference frame.

We command a force through a linear force actuator at the prismatic joint of each leg. This is given by

$$\vec{F}^A_i = \frac{|\vec{N}_{iL}|}{(\hat{n}_i \cdot \hat{f}^A_i)}\hat{f}^A_i \tag{10}$$

where $\hat{f}^A_i$ is the unit vector in the direction of the actuator force given by $\hat{f}^A_i = R\begin{bmatrix} 0 & 0 & 1 \end{bmatrix}^T$

2.2. Determination of net forces and moments on the chassis

Remark: Along the sliding direction of the prismatic joint the only force to be considered is the commanded actuator force ($\vec{F}^A_i$). Assuming the suspension system of the LFA-V1 to be an ideal suspension system, the property of a prismatic joint with linear force actuator is that only the components of $\vec{T}_i$ and $\vec{N}_i$ perpendicular to $\vec{F}^A_i$ get transmitted to the chassis. So the forces are decomposed into two parts: one along the direction of the actuator and the other along the direction perpendicular to the actuator. The forces along the actuator are discarded since they are not transmitted to the chassis and only the forces perpendicular to the chassis are considered in the analysis.

To find the components of $\vec{T}_i$ perpendicular to $\vec{F}^A_i$, $\vec{R}_{tai}$, which is resulted when $\hat{f}^A_i$ is rotated by $\pi/2$ radians towards $\hat{t}_i$ about $\vec{K}_{ti} = (\hat{t}_i \times \hat{f}^A_i)$ is determined [7] and is given by

$$\vec{R}_{tai} = R_{K_{ti}}\left(\frac{\pi}{2}\right)\hat{f}^A_i \tag{11}$$

where

$$\frac{\vec{K}_{ti}}{|\vec{K}_{ti}|} = \begin{bmatrix} k_{txi} & k_{tyi} & k_{tzi} \end{bmatrix}^T$$

$$R_{K_{ti}}\left(\frac{\pi}{2}\right) = \begin{bmatrix} k_{txi}^2 & k_{txi}k_{tyi} - k_{tzi} & k_{txi}k_{tzi} + k_{tyi} \\ k_{txi}k_{tyi} + k_{tzi} & k_{tyi}^2 & k_{tyi}k_{tzi} - k_{txi} \\ k_{txi}k_{tzi} - k_{tyi} & k_{tyi}k_{tzi} + k_{txi} & k_{tzi}^2 \end{bmatrix}$$

$$\text{and } \frac{\vec{K}_{ti}}{\left|\vec{K}_{ti}\right|} = \begin{bmatrix} k_{txi}k_{tyi}k_{tzi} \end{bmatrix}^T \tag{12}$$

Hence, the net traction force in the direction perpendicular to the actuator force is given by

$$\vec{T}_{neti} = (\hat{t}_i \cdot \vec{R}_{tai})|\vec{T}_i|\vec{R}_{tai} \tag{13}$$

Similarly to find the components of $\vec{N}_i$ perpendicular to $\vec{F}^A_i$, $\vec{R}_{nai}$ is determined, which is resulted when $\hat{f}^A_i$ is rotated by $\pi/2$ radians towards $\hat{n}_i$ about the vector $\vec{K}_{ni} = (\hat{n}_i \times \hat{f}^A_i)$

$$\vec{R}_{nai} = R_{K_{ni}}\left(\frac{\pi}{2}\right)\hat{f}^A_i \tag{14}$$

Please cite this article as: V.P. Eathakota, et al., Two models of force actuator based active suspension mechanisms for mobility on uneven terrain, Acta Astronautica (2010), doi:10.1016/j.actaastro.2010.06.051

where

$$R_{K_{ni}}\left(\frac{\pi}{2}\right)=\begin{bmatrix} k_{nxi}^2 & k_{nxi}k_{nyi}-k_{nzi} & k_{nxi}k_{nzi}+k_{nyi} \\ k_{nxi}k_{nyi}+k_{nzi} & k_{nyi}^2 & k_{nyi}k_{nzi}-k_{nxi} \\ k_{nxi}k_{nzi}-k_{nyi} & k_{nyi}k_{nzi}+k_{nxi} & k_{nzi}^2 \end{bmatrix}$$

$$\text{and } \frac{\vec{K}_{ni}}{|\vec{K}_{ni}|}=\begin{bmatrix} k_{nxi} & k_{nyi} & k_{nzi} \end{bmatrix}^T \tag{15}$$

Hence, the net normal force in the direction perpendicular to the actuator force is given by

$$\vec{N}_{neti}=(\hat{n}_i\cdot\vec{R}_{nai})|\vec{N}_i|\vec{R}_{nai} \tag{16}$$

Thus, the net force and moment $(\vec{F},\vec{M})$ acting on the chassis of the vehicle is given by the vector sum

$$\vec{F}=\sum_{i=1}^{4}(\vec{F}_i^A+\vec{T}_{neti}+\vec{N}_{neti})+m\vec{g} \tag{17}$$

$$\vec{M}=\sum_{i=1}^{4}[(\vec{r}_{fai}\times\vec{F}_i^A)+\vec{r}_{tni}\times(\vec{T}_{neti}+\vec{N}_{neti})] \tag{18}$$

where m is the mass of the chassis, $\vec{g}$ the acceleration due to gravity, $\vec{r}_{fai}$ the radius vector from the ith leg to the CG of the chassis and $\vec{r}_{tni}$ the radius vector from the point of contact of the ith wheel to the CG of the chassis. The unit vector corresponding to the net normal and traction forces are given by

$$\hat{t}_{neti}=\frac{\vec{T}_{neti}}{|\vec{T}_{neti}|}=\begin{bmatrix} t_{netxi} & t_{netyi} & t_{netzi} \end{bmatrix}^T$$

$$\hat{n}_{neti}=\frac{\vec{N}_{neti}}{|\vec{N}_{neti}|}=\begin{bmatrix} n_{netxi} & n_{netyi} & n_{netzi} \end{bmatrix}^T \tag{19}$$

$\vec{r}_{tni}$ is given by $\vec{r}_{tni}=\vec{r}_{fai}+\vec{r}_1+\vec{r}_2+\vec{r}_3$ where

$$\vec{r}_{fai}=R\left[\frac{(2.5-i)}{|(2.5-i)|}W(-1)^{i+1}L0\right]^T\ \forall\, i=\{1,2,3,4\}$$

$2L$ is the length of the chassis and $2W$ the width of the chassis

$$\vec{r}_1=R\begin{bmatrix} 0 & 0 & -l_i \end{bmatrix}^T,\quad \vec{r}_2=R\begin{bmatrix} 0 & -r\sin(\gamma_i) & -r\cos(\gamma_i) \end{bmatrix}^T,$$

$$\gamma_i\approx\tan^{-1}(N_{yi}/N_{zi}),\quad \vec{r}_3=-r_t\hat{n}_i$$

where l_i is the length of the ith leg, r the radius of the wheels, r_t the radius of the torus cross section and γ_i the slope in the sagittal plane.

Let $\begin{bmatrix} m_{txi} & m_{tyi} & m_{tzi} \end{bmatrix}^T$, $\begin{bmatrix} m_{nxi} & m_{nyi} & m_{nzi} \end{bmatrix}^T$ be the unit moment vectors due to $\vec{T}_i$ and $\vec{N}_i$, respectively.

Hence from Eqs. (17)–(19) the quasi-static equations that relate the normal and traction forces to the forces on the chassis of a three dimensional (3D) four-wheeled LFA-V1 can be put in the form

$$\overline{A}\cdot\overline{C}=\overline{D} \tag{20}$$

where

$$\overline{C}=\begin{bmatrix} |\vec{T}_1| & |\vec{N}_1| & |\vec{T}_2| & |\vec{N}_2| & |\vec{T}_3| & |\vec{N}_3| & |\vec{T}_4| & \vec{N}_4 \end{bmatrix}^T$$

$$\overline{D}=\begin{bmatrix} F_x & F_y & F_z & M_x & M_y & M_z \end{bmatrix}^T$$

$$\overline{A}=\begin{bmatrix} t_{netx1} & n_{netx1} & t_{netx2} & n_{netx2} & t_{netx3} & n_{netx3} & t_{netx4} & n_{netx4} \\ t_{nety1} & n_{nety1} & t_{nety2} & n_{nety2} & t_{nety3} & n_{nety4} & t_{nety4} & n_{nety4} \\ t_{netz1} & n_{netz1} & t_{netz2} & n_{netz2} & t_{netz3} & n_{netz3} & t_{netz4} & n_{netz4} \\ m_{tx1} & m_{nx1} & m_{tx2} & m_{nx2} & m_{tx3} & m_{nx3} & m_{tx4} & m_{nx4} \\ m_{ty1} & m_{ny1} & m_{ty2} & m_{ny2} & m_{ty3} & m_{ny3} & m_{ty4} & m_{ny4} \\ m_{tz1} & m_{nz1} & m_{tz2} & m_{nz2} & m_{tz3} & m_{nz3} & m_{tz4} & m_{nz4} \end{bmatrix}$$

From the quasi-static analysis of the LFA-V1 it is observed that to achieve a stable posture for the vehicle the parameters that need to be controlled while traversing a terrain are the height h of the chassis, its pitch ψ, roll α and yaw β about the global $\{XYZ\}$ axes. To achieve required acceleration for the vehicle in the Y, F_y is commanded.

2.3. Controlling the moments and forces for stable posture

A stable posture can be achieved by defining F_z, M_x, M_y, M_z depending on the set of parameters h, ψ, α and β as

$$F_z=k_pe_h+k_v\dot{e}_h+mg,\quad M_x=\overline{k}_pe_\psi+\overline{k}_v\dot{e}_\psi$$
$$M_y=\hat{k}_pe_\alpha+\hat{k}_v\dot{e}_\alpha,\quad M_z=\tilde{k}_pe_\beta+\tilde{k}_v\dot{e}_\alpha \tag{21}$$

where

$$e_h=h_d-h,\quad e_\psi=\psi_d-\psi$$
$$e_\alpha=\alpha_d-\alpha,\quad e_\beta=\beta_d-\beta \tag{22}$$

are the differences between the desired values and the instantaneous values of the parameters being controlled and $k_p,\overline{k}_p,\hat{k}_p,\tilde{k}_p$ and $k_v,\overline{k}_v,\hat{k}_v,\tilde{k}_v$ are the proportional and derivative gains, respectively, to maintain stable posture. The control equation of (21) and (22) helps in controlling the posture error that could grow rapidly due to differences between the vehicle model as modeled by the quasi-static framework versus the actual model of the vehicle. These differences arise among other things due to the assumptions of negligible link mass when compared with the main body and can result in pitching or rolling of the vehicle that is compensated by the control laws. To depict the force controllability of the LFA-V1 consider the following optimization problem:

$$\min(S),S=\sum_{i=1}^{4}|\vec{T}_i| \tag{23}$$

Subject to the equality constraints (20) and the set of inequality constraints given by

$$|\vec{N}_i|>0,\quad \forall i=\{1,2,3,4\} \tag{24}$$

$$|\vec{T}_i|<\mu_i|\vec{N}_i|,\quad \forall i=\{1,2,3,4\} \tag{25}$$

$$\Gamma_i^{min}\le(|\vec{T}_i|r)\le\Gamma_i^{max},\quad \forall i=\{1,2,3,4\} \tag{26}$$

$$|\vec{F}_i^A|\le F_{ub} \tag{27}$$

$$|\vec{T}_i|\ge|\vec{F}_i^A\cdot\vec{T}_i|+|\overrightarrow{W}_i\cdot\vec{T}_i|,\quad \forall i=\{1,2,3,4\} \tag{28}$$

Please cite this article as: V.P. Eathakota, et al., Two models of force actuator based active suspension mechanisms for mobility on uneven terrain, Acta Astronautica (2010), doi:10.1016/j.actaastro.2010.06.051

where (24) corresponds to the constraint that the wheel maintains contact with the ground always, (25) corresponds to the no-slip constraint and (26) corresponds to the constraint that the torque required to generate the required traction is between Γ_i^{min} and Γ_i^{max}, (27) corresponds to the fact the there is an upper bound on the amount of actuator force that can be generated and is given by F_{ub}. Constraint (28) comes from analyzing the free body diagram of the wheel as shown in Fig. 4c. For the wheel to climb a given slope γ_i, the traction force should be greater than the component of the actuator force and the weight ($\overrightarrow{W}_i$) of the wheel along the traction direction. This follows from the inherent characteristics of the LFA-V1, which allows for the wheel to have dynamics in the vertical direction independent of the movement of the chassis. The above optimization problem (23) is solved for the values of the traction and normal forces $(\overrightarrow{T}_i, -N_i) \forall i = \{1,2,3,4\}$ with the above set of equality and inequality conditions. It is assumed that both the rear wheels have the same contact angle γ_2 and both the front wheels have contact angle γ_1. γ_2 is set to 0 and γ_1 is varied from 0° to 90° and the pitch angle ψ from 0° to 60° to evaluate the regions of feasible and infeasible solutions to the above optimization problem.

Fig. 5 shows the plot of min(S) as a function of the contact angle γ_1 pitch ψ. The maximum motor torque ratings were set at 2 Nm for each wheel and the upper bound for F_{ub} is 60 N (which can be achieved by available industrial actuators [12]) and the weight of the vehicle was taken to be 8.5 kg. From Figs. 5 and 6 it can be observed that for contact angles greater than 40° there arise regions for which no solution for the above optimization problem exists, i.e. the vehicle cannot climb slopes greater than 40°. The reason for this being the violation of constraint (28) and this is unique to our vehicle. For slope angles greater than 40° the downward component of vertical actuator force and the weight of the wheel in the direction of the traction force becomes greater than the magnitude of the traction force. Moreover, as slope angle increases to values close to 90° the component of vertical actuator force along the normal force direction given by $(\overrightarrow{F}_i^A \cdot \overrightarrow{N}_i)\overrightarrow{N}_i$ also reduces considerably

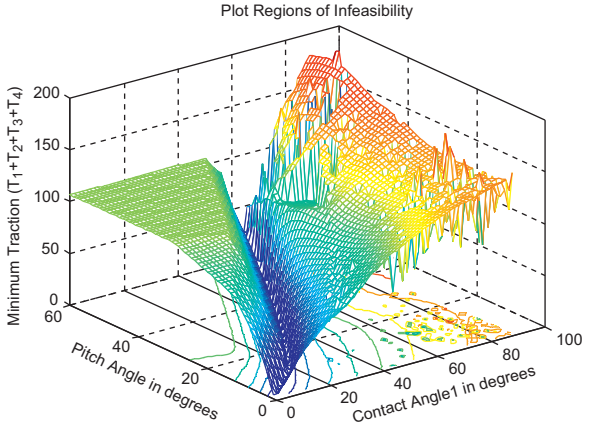

Fig. 5. Plot showing regions of infeasibility for LFA-V1.

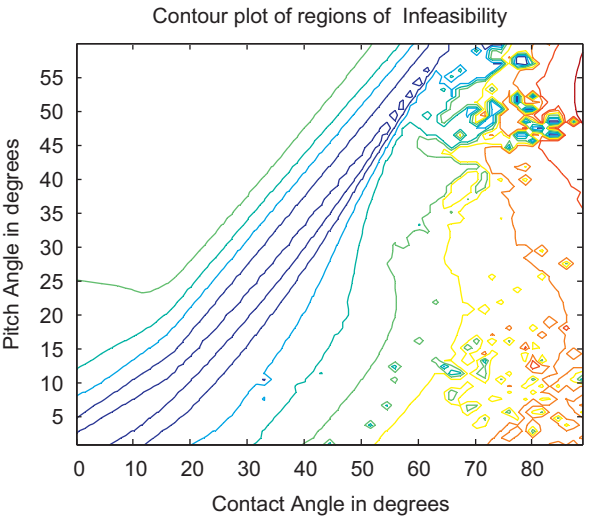

Fig. 6. Contour plot of regions of infeasibility for LFA-V1.

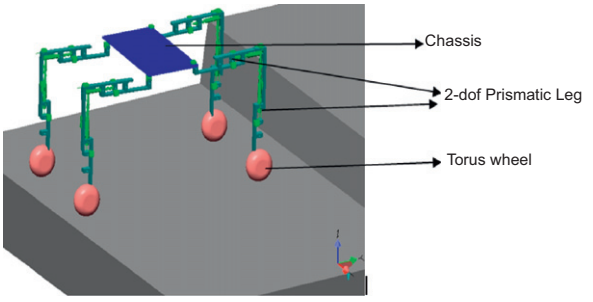

Fig. 7. The LFA-V2 mechanical structure.

leading to the reduction in the generated normal force and hence further reducing traction and increasing the chances of violation of constraint (28). To overcome this a modified mechanism of the LFA-V having a 2-*dof* actuated leg is developed, which will be discussed in the next section.

3. Quasi-static analysis of LFA-V2

As discussed in the above section to adapt to discontinuous surfaces and terrains having higher slope angles a modified design for the above vehicle (shown in Fig. 7) is developed and is called the LFA-V2 to signify that each leg of the vehicle has now 2 degrees of freedom as compared to 1 in the previous design. Fig. 8 shows the conceptual model of the modified leg. The horizontal portion of the leg is exactly similar to the vertical legs of LFA-V1. Each leg of the LFA-V2 has 2 actuated prismatic joints, which are connected rigidly in a mutually orthogonal fashion with each other. The vertical and the horizontal prismatic joints are similar to that of the LFA-V1. Fig. 9 shows the parallel manipulator equivalent of the LFA-V2. Using (1) we have N to be 22 (four parts comprising two linear actuator pairs and wheel for each leg and the ground and the chassis), J is equal to 24 (1 joint connecting the wheel and 2 prismatic joints and 2

Please cite this article as: V.P. Eathakota, et al., Two models of force actuator based active suspension mechanisms for mobility on uneven terrain, Acta Astronautica (2010), doi:10.1016/j.actaastro.2010.06.051

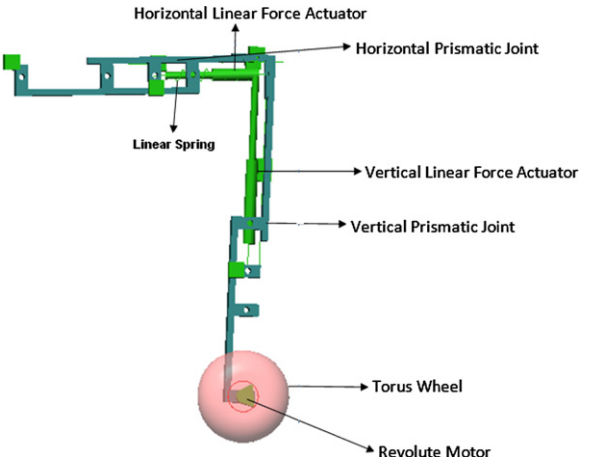

Fig. 8. The LFA-V2 actuated leg.

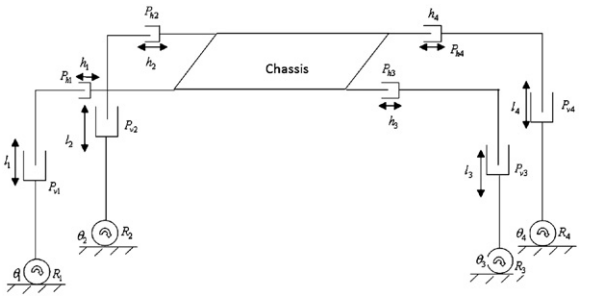

Fig. 9. The LFA-V2 as a parallel manipulator.

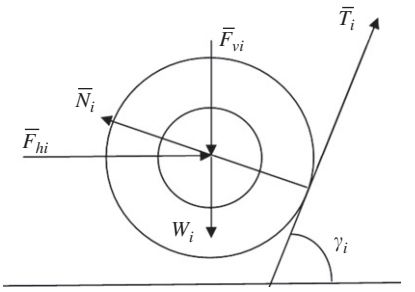

Fig. 10. FBD of the wheel for a LFA-V2.

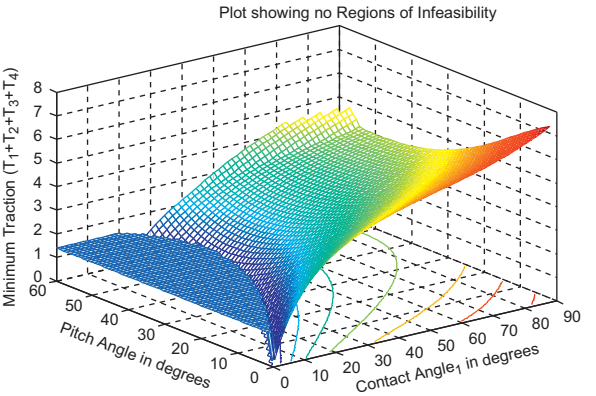

Fig. 11. Plot showing NO regions of infeasibility for LFA-V2.

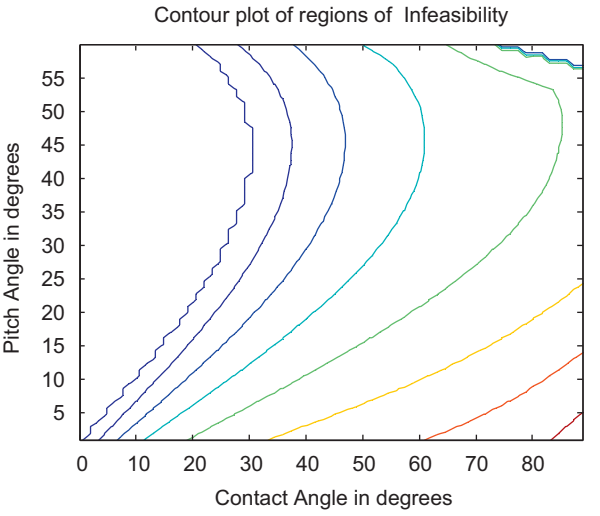

Fig. 12. Contour plot showing NO regions of infeasibility for 2-*dof* LFA-V.

rigid joints connecting the horizontal and the vertical prismatic pairs and the horizontal prismatic pair with the chassis and 4 wheel–ground contact points) and $\sum_{i=1}^{J} F_i$ is equal to 24 (2 prismatic and 1 rotational joint for each leg and 3 *dof* joints at each wheel–ground contact point with ideal rolling constraint and the connection between the horizontal and the vertical prismatic pairs and between the horizontal prismatic pairs and the chassis are rigid with 0 *dof*) and hence overall *dof* of the system is 6. But similar to the LFA-V1, this is also a redundantly actuated vehicle with 12 actuated joints. Between the joints where the horizontal actuator force is connected we also have linear springs. They serve two main purposes: first they act as shock absorbers if the vehicle suddenly encounters a discontinuity similar to any vehicle suspension system. Second the horizontal actuators are used only at times where there is a 2 point contact between the wheel and the terrain. It is assumed here that the vehicle is running on non-continuous surfaces and slopes greater than 40° will invariably result in 2 point contact between the wheel and the terrain, which can be predicted if the vehicle is equipped with wheels as proposed in [14]. Lower slope angles in the order of less than 40° can be negotiated by LFA-V1 as shown by the feasibility plot and hence there is no necessity to activate the second actuator. In such situations linear springs passively control the horizontal prismatic joint.

3.1. Calibration of the horizontal actuator force

Consider the FBD of the wheel as shown in Fig. 10. There are 3 forces acting on the *i*th wheel. The normal force $\vec{N}_i$, the traction force $\vec{T}_i$, the vertical actuator force $\vec{F}_{vi}$, which is always perpendicular to the chassis

Please cite this article as: V.P. Eathakota, et al., Two models of force actuator based active suspension mechanisms for mobility on uneven terrain, Acta Astronautica (2010), doi:10.1016/j.actaastro.2010.06.051

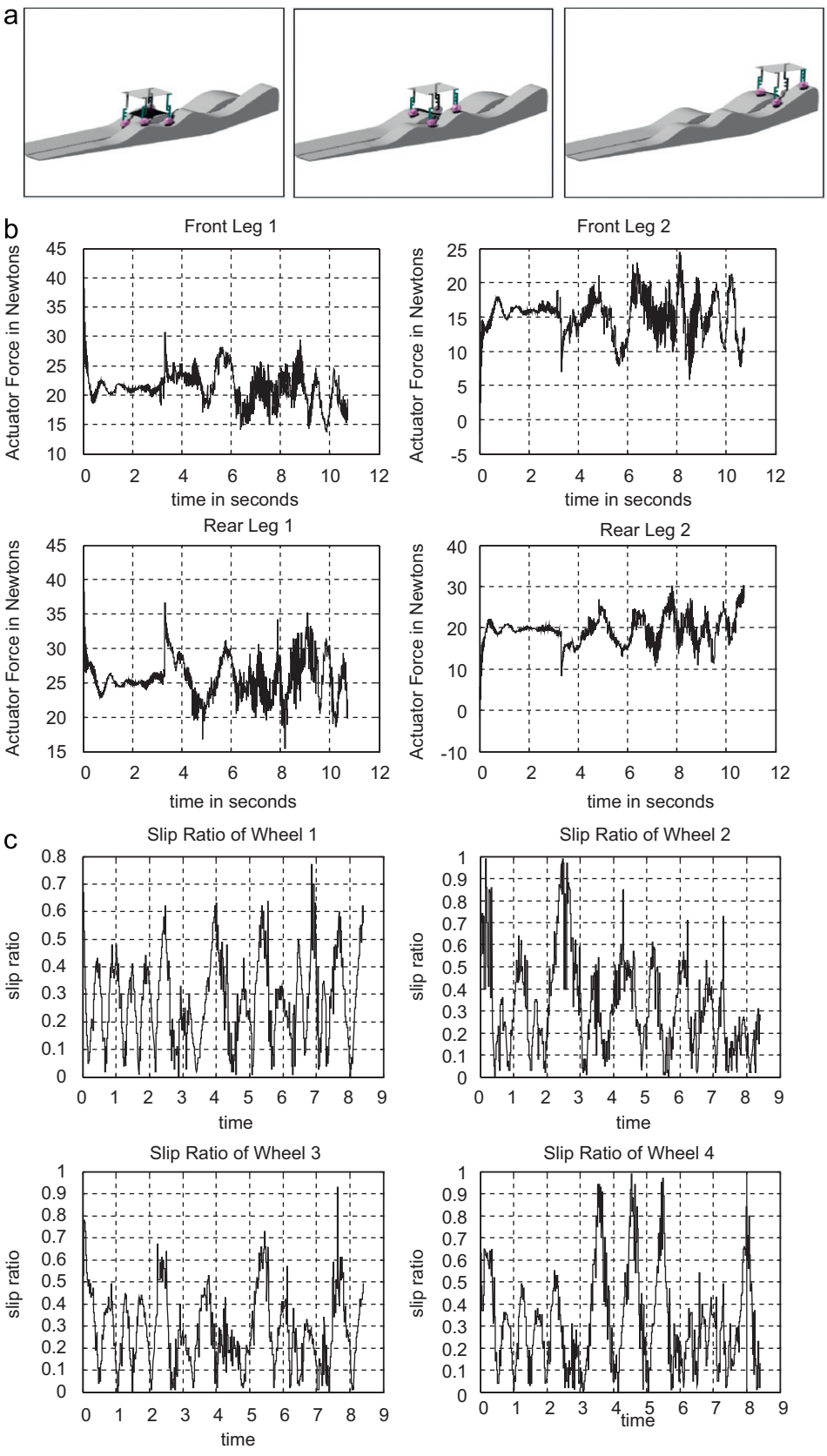

Fig. 13. (a) LFA-V1 negotiating a sample terrain. (b) LFA-V1 actuator forces plot in Newtons. (c) LFA-V1 the slip ratio of each wheel. (d) LFA-V1 velocity of the chassis in m/s. (e) LFA-V1 negotiating a fully 3D terrain. (f) LFA-V1 actuator forces plot in Newtons for fully 3D terrain. (g) LFA-V1 slip ratio of each wheel for fully 3D terrain. (h) LFA-V1 velocity of the chassis in m/s for fully 3D terrain.

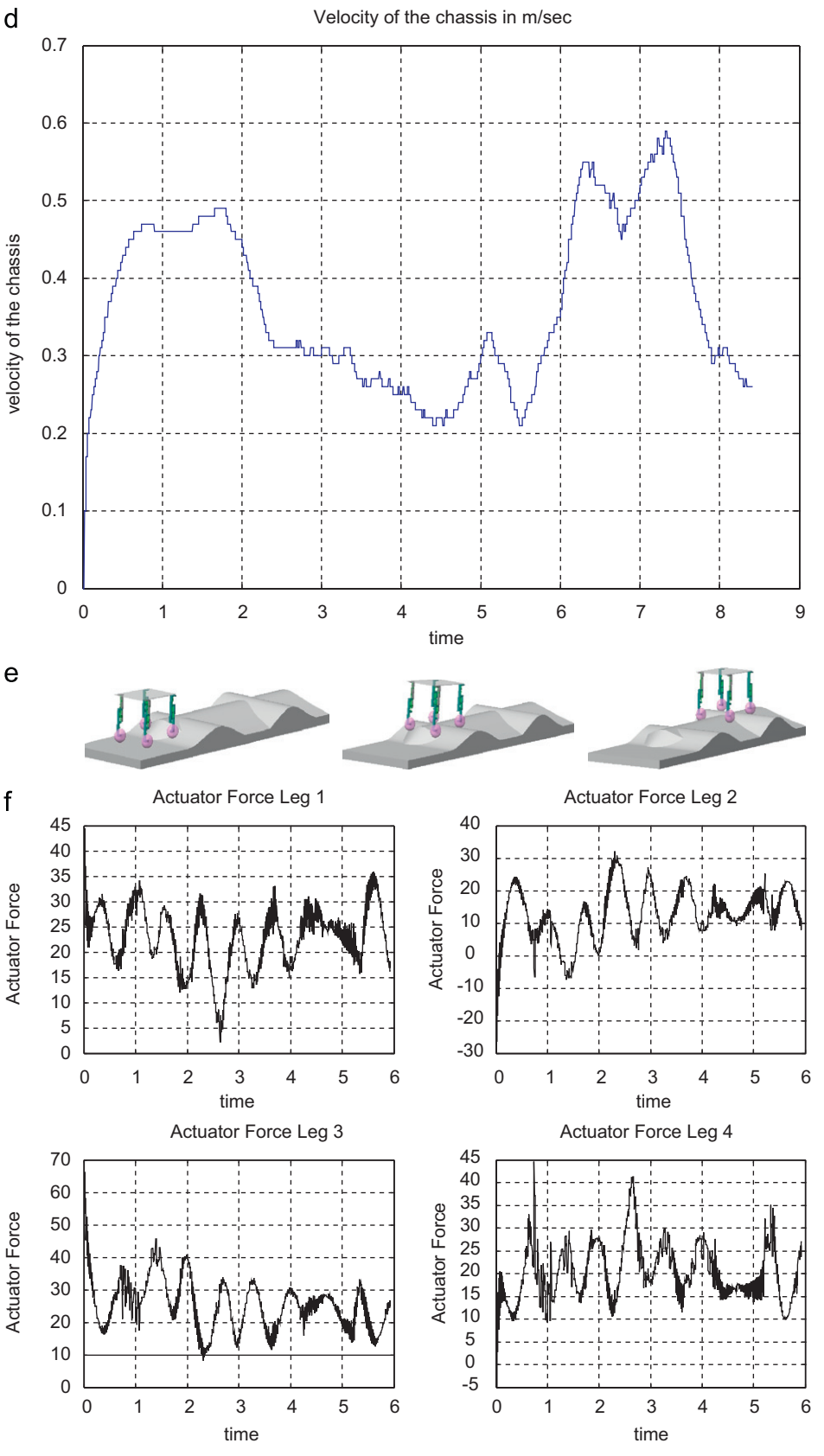

Fig. 13. (*Continued*)

Please cite this article as: V.P. Eathakota, et al., Two models of force actuator based active suspension mechanisms for mobility on uneven terrain, Acta Astronautica (2010), doi:10.1016/j.actaastro.2010.06.051

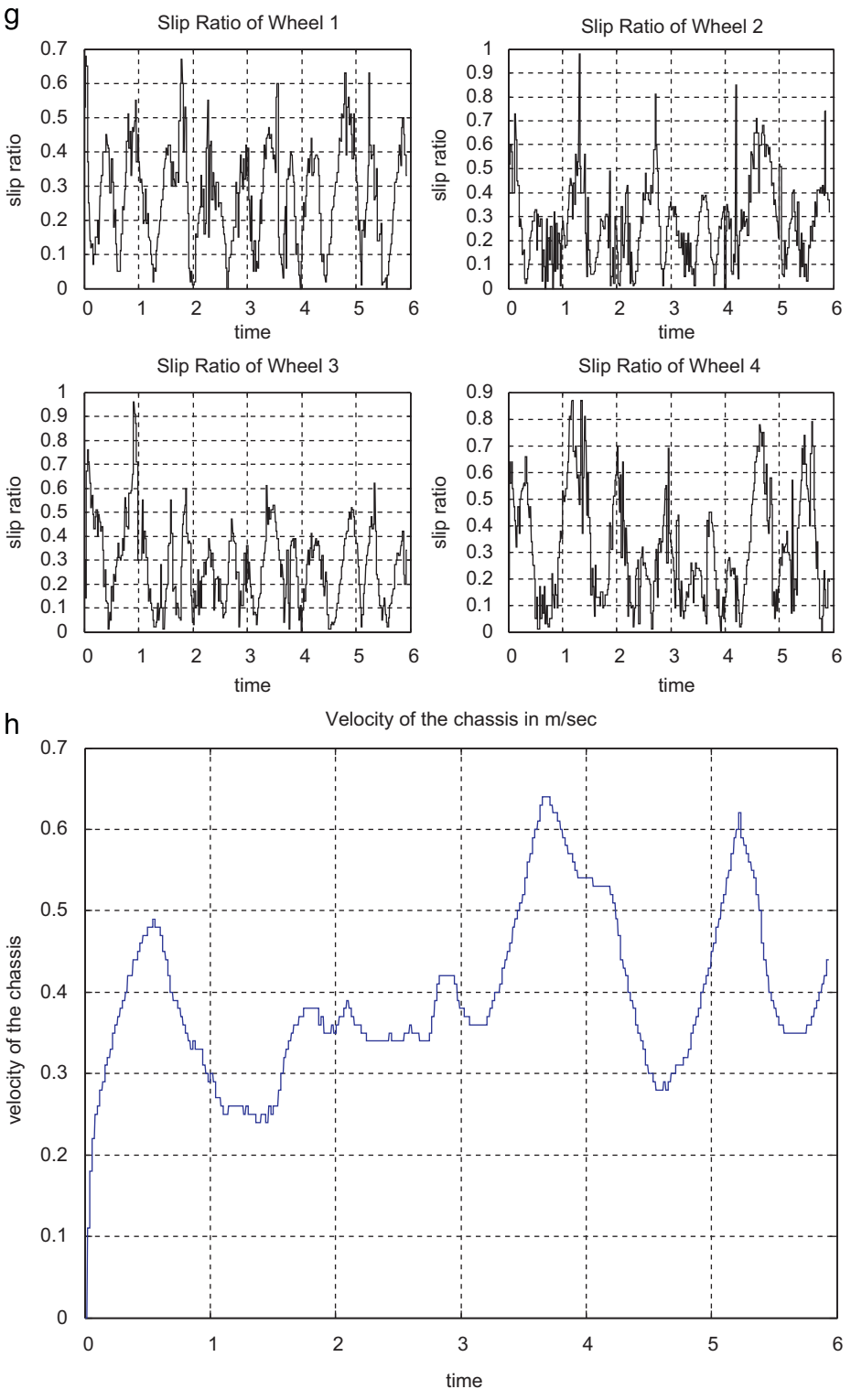

Fig. 13. (*Continued*)

and the horizontal actuator force $\vec{F}_{hi}$ and the weight of the wheel $\vec{W}_i$.

The horizontal actuator force is such that it balances the vertical actuator force and the component of the weight of the wheel in the direction of the traction force $\vec{T}_i$ and the spring stiffness.

$$|\vec{F}_{hi}\cdot\vec{T}_i| = |\vec{F}_{vi}\cdot\vec{T}_i| + |\vec{W}_i\cdot\vec{T}_i| + |\vec{K}| \quad (29)$$

Please cite this article as: V.P. Eathakota, et al., Two models of force actuator based active suspension mechanisms for mobility on uneven terrain, Acta Astronautica (2010), doi:10.1016/j.actaastro.2010.06.051

where $\vec{K}$ denotes component of the vector of the force generated by the stiffness of the springs along the traction direction and $\vec{K} = sx + c(dx/dt)$ where s is the spring constant, c the damping coefficient and x denotes the change in length of the spring. s and c are assumed to be the known properties of the springs and x and dx/dt can be estimated easily by appropriate sensors. Also $\vec{F}_{vi} = \vec{F}^{A}_{i}$, which is the same as the actuator force in the LFA-V1 case. Hence, we have

$$|\vec{F}_{hi}| = \frac{|\vec{F}_{vi}|[R[0 \quad 0 \quad 1]^T]^T\hat{t}_i + |\vec{W}_i|[R[0 \quad 0 \quad 1]^T]^T\hat{t}_i}{[R[0 \quad 0 \quad 1]^T]^T\hat{t}_i} + |\vec{K}| \tag{30}$$

where $\vec{K}$ is a stiffness force of the springs, which can be estimated at each instant since the constraint spring length and rate of change of length can be estimated with the help of appropriate sensors. Hence, the net force and moments $(\vec{F}, \vec{M})$ acting on the chassis can be derived using a similar procedure as that of the LFA-V1 and are given by

$$\vec{F} = \sum_{i=1}^{4}[\vec{T}_{neti} + \vec{N}_{neti} + \vec{F}_{hi}]$$

$$\vec{M} = \sum_{i=1}^{4}[(\vec{r}_{hi} \times \vec{F}_{hi}) + \vec{r}_{hi} \times (\vec{T}_{neti} + \vec{N}_{neti})] \tag{31}$$

where $\vec{r}_{hi} = R\begin{bmatrix} l/2 & 0 & 0 \end{bmatrix}^T$ where l is the length of the chassis in the global X direction.

Hence, using a similar procedure to that of the LFA-V1 we can get a similar quasi-static equation given by

$$\overline{A}_2 \cdot \overline{C} = \overline{D} \tag{32}$$

3.2. Change in constraint (28) due to horizontal actuator

Since the component of horizontal actuator force along the traction direction exactly balances the downward component of vertical actuator force along the traction direction, we have a modified FBD of the wheel as shown in Fig. 10 where a new force due to the horizontal actuator has come into picture. As can be seen from Fig. 10 the condition for the wheel to move up the slope, which is given by

$$|\vec{T}_i| \geq |\vec{W}_i \cdot \vec{T}_i| \tag{33}$$

To demonstrate the force controllability of the LFA-V2 the optimization problem (23) is solved subject to the

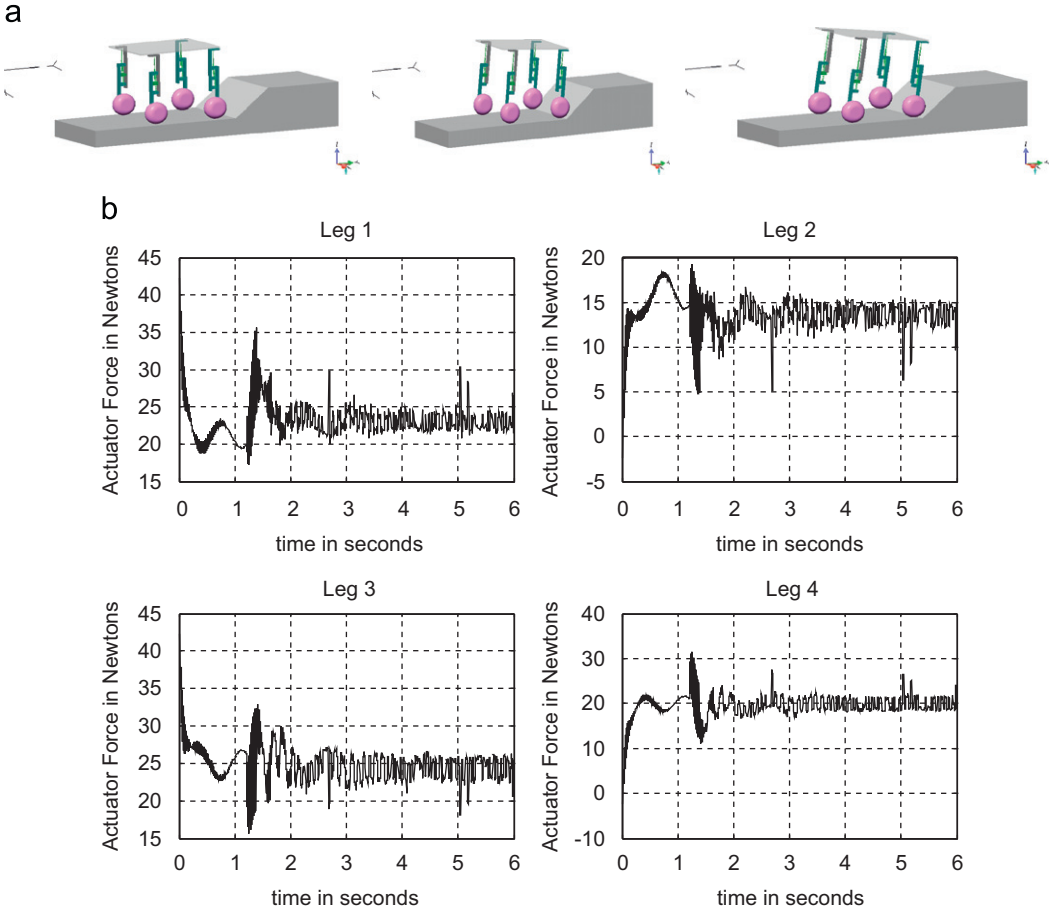

Fig. 14. (a) LFA-V1 unable to negotiate a 40^0 slope. (b) LFA-V1 plot of actuator forces in Newtons.

Please cite this article as: V.P. Eathakota, et al., Two models of force actuator based active suspension mechanisms for mobility on uneven terrain, Acta Astronautica (2010), doi:10.1016/j.actaastro.2010.06.051

new equality constraint given in (32) and the inequality constraints (24) through (27) and modified constraint (33). It is assumed that both the rear wheels have the same contact angle γ_2 and both the front wheels have contact angle γ_1. γ_2 is set to 0, and γ_1 is varied from 0° to 90° and the pitch angle ψ from 0° to 60° to evaluate the regions of feasible and infeasible solutions to the above optimization problem. Fig. 11 shows the plot of min(S) as a function of the contact angle γ_1 pitch ψ. The maximum motor torque ratings were set at 2 N m for each wheel and the upper bound for F_{ub} is 60 N and the weight of the vehicle was taken to be 8.5 kg. As can be seen from Figs. 11 and 12 the regions of infeasible solutions have been completely eliminated for the case of LFA-V2. This is mainly because of the presence of the horizontal force actuator, which enables us to overcome the constraint (28).

4. Simulations and results

To demonstrate the mobility of our vehicles we perform all the simulations in a dynamic physics engine (MSC VisualNastran) using the MATLAB/SIMULINK interface. The simulations were tested with an integration time step of 0.004 s for LFA-V1 and 0.05 s for LFA-V2. Fig. 13a shows the LFA-V1 negotiating a sample terrain having each leg at a different heights at any instant. Fig. 13b is the corresponding plot of the actuator forces. Fig. 13c

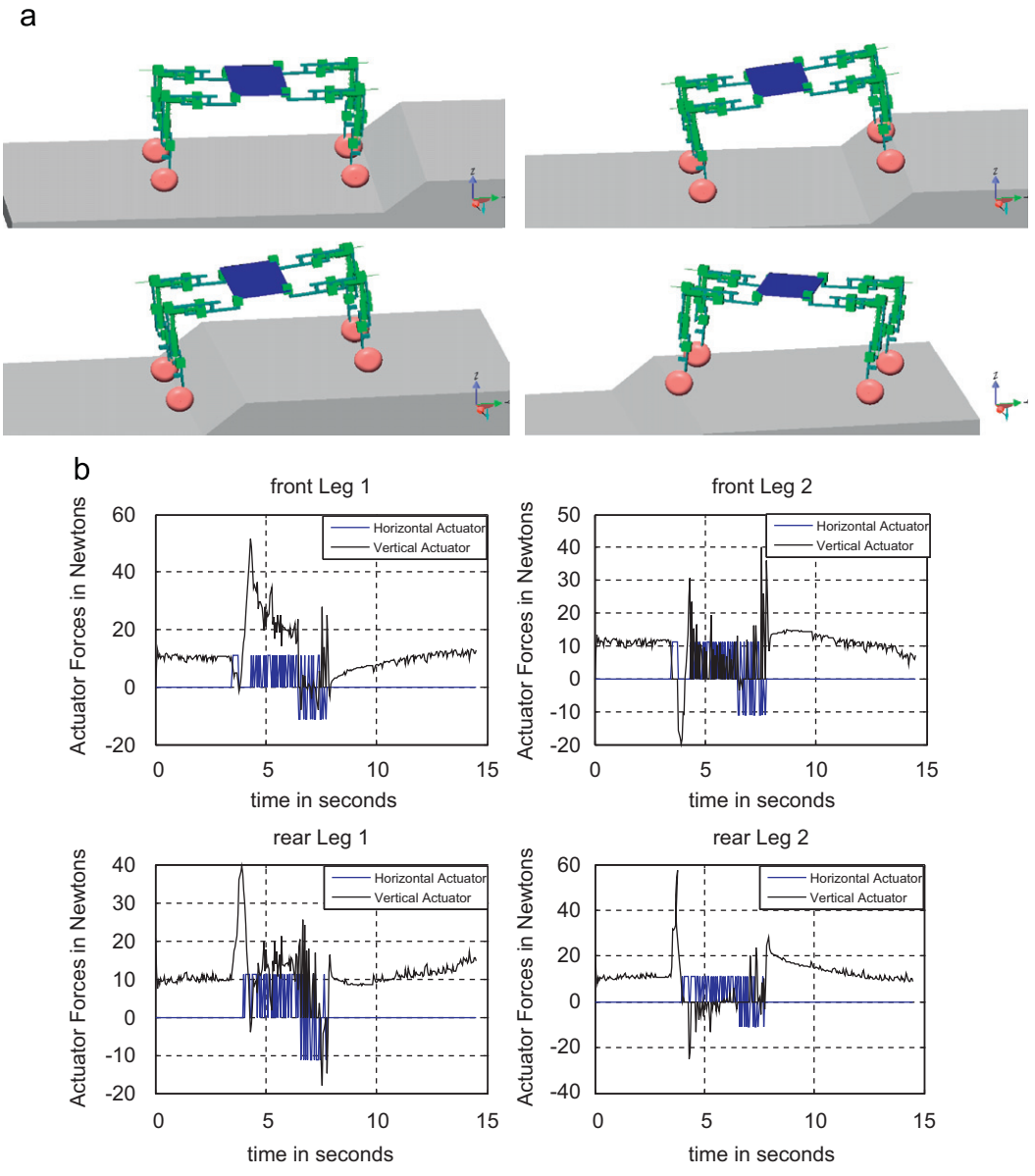

Fig. 15. (a) LFA-V1 negotiating a 40° slope. (b) LFA-V2 actuator forces plot in Newtons.

Please cite this article as: V.P. Eathakota, et al., Two models of force actuator based active suspension mechanisms for mobility on uneven terrain, Acta Astronautica (2010), doi:10.1016/j.actaastro.2010.06.051

shows the plot of the absolute value of the slip ratio of each of the wheels of the vehicle in which wheels 1 and 2 correspond to the front wheels and the wheels 3 and 4 correspond to the rear wheels. Fig. 13d shows the plot of the velocity of the chassis during the simulation and it can be observed that the vehicle is moving considerably slow with a maximum velocity of 0.6 m/s and hence the quasi-static analysis is valid. In the plot shown in Fig. 13c the peak of the slip ratio for wheels 2 and 4 occurs at the instant when wheels 1 and 3 are crossing a slope, respectively, and wheels 2 and 4 are on relatively flat terrain. Fig. 13(e–h) shows the similar plots for the LFA-V1 negotiating a fully 3D terrain. It can be observed from the plots that the vehicle is moving considerably slow with a maximum velocity of 0.65 m/s and hence the quasi-static analysis can be considered to be valid. The slip-ratio plot shown in Fig. 13g shows a more uniform variation in the slip ratio and can be attributed to the terrain profile. The average values of the slip ratio for both the terrains remain within 0.4–0.6. Fig. 14a shows the LFA-V1 is unable to climb a 40° slope because the developed traction force cannot overcome the downward component of vertical actuator force which pushes the wheel downward and as can be seen from Fig. 14b the actuator forces settle down to a finite value. Fig. 15a shows the LFA-V2 negotiating a 40° slope. In this case as can be seen from Fig. 15b whenever a 2 point contact occurs the corresponding horizontal actuators come into action, which balance the downward component of vertical actuator force and also have a positive component along the normal force direction, which further results in the net increase in the traction force as

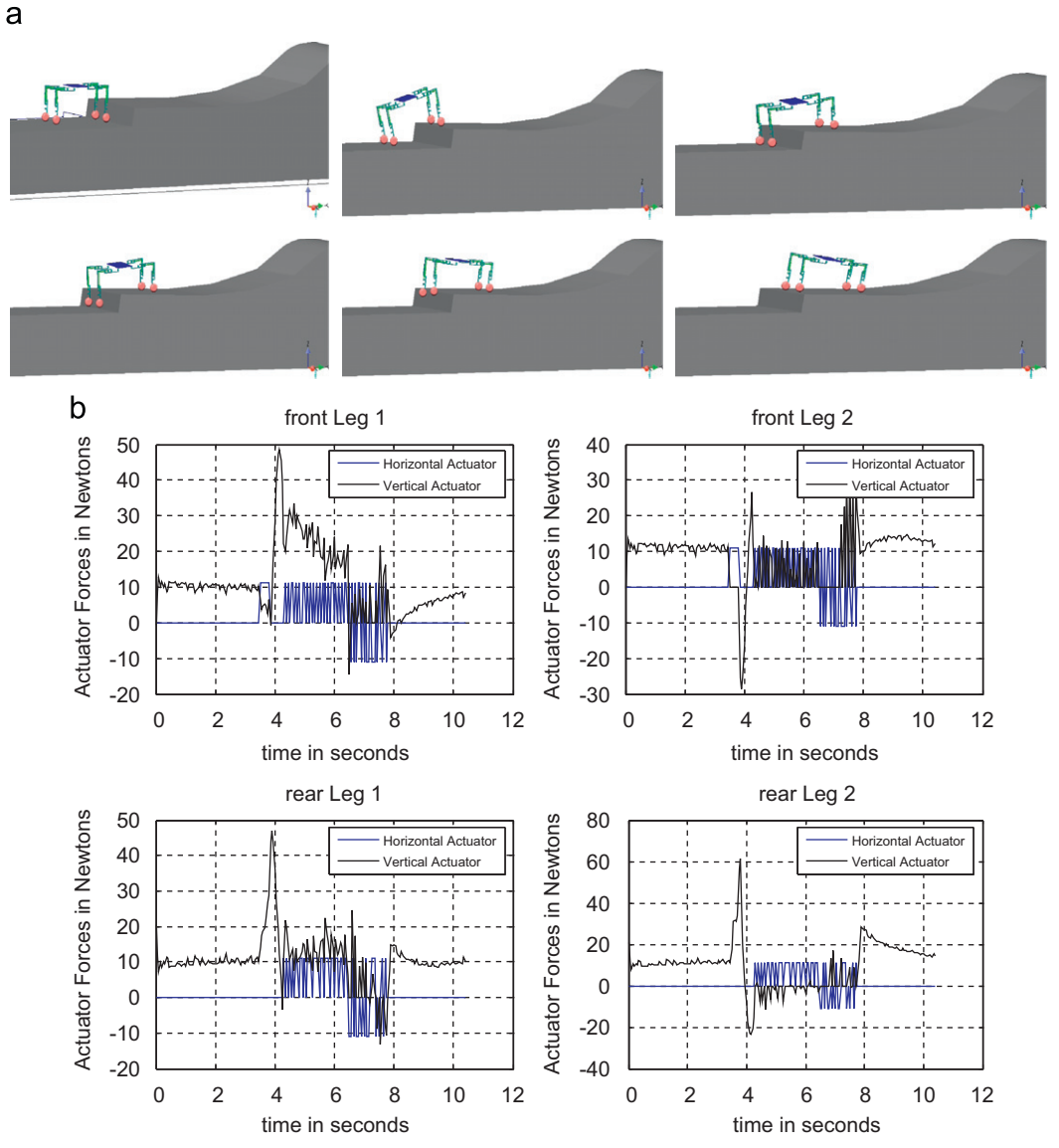

Fig. 16. (a) LFA-V2 on a sample terrain. (b) LFA-V2 plot of actuator forces in Newton. (c) LFA-V2 slip ratio for the simulation of the above terrain. (d) LFA-V2 the velocity of the chassis in m/s.

Please cite this article as: V.P. Eathakota, et al., Two models of force actuator based active suspension mechanisms for mobility on uneven terrain, Acta Astronautica (2010), doi:10.1016/j.actaastro.2010.06.051

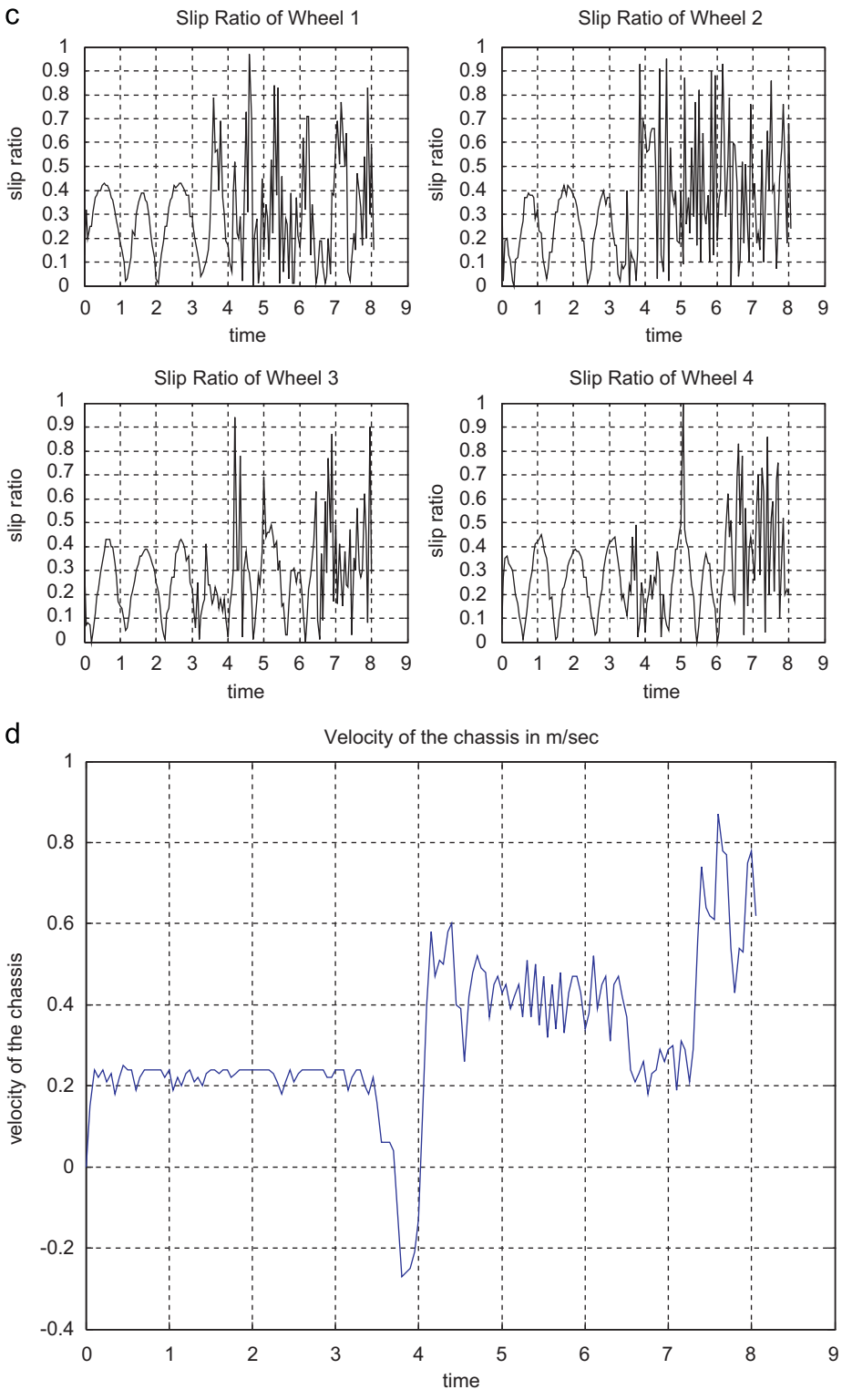

Fig. 16. (*Continued*)

was discussed with the help of the FBD of the wheel (Fig. 10). Fig. 16a shows the LFA-V2 negotiating a sample terrain. The initial discontinuity in the terrain is 2 times the wheel diameter. Fig. 16b shows the plots of the horizontal and vertical actuator forces. As can be seen from the figures the horizontal actuators get activated

Please cite this article as: V.P. Eathakota, et al., Two models of force actuator based active suspension mechanisms for mobility on uneven terrain, Acta Astronautica (2010), doi:10.1016/j.actaastro.2010.06.051

Table 1
Summary of parameters resulting from the simulation.

Simulation	Coefficient of friction (μ)	Maximum linear actuator force	Maximum linear actuator length	Maximum motor torque	Maximum slope angle	Remarks
Fig. 13a	0.5	Vertical—35 N Horizontal —	Vertical—0.58 m Horizontal —	1.2 N m	25°	Traversable
Fig. 14a	0.5	Vertical—45 N Horizontal —	Vertical—0.65 m Horizontal —	1.8 N m	40°	Not-traversable
Fig. 15a	0.5	Vertical—58 N Horizontal—10 N	Vertical—0.35 m Horizontal—0.21 m	1.2 N m	40°	Traversable
Fig. 16a	0.8	Vertical—60 N Horizontal—10 N	Vertical—0.4 m Horizontal—0.25 m	1.95 N m	85°	Traversable

only when a 2 point contact occurs (in this case when the discontinuity occurs). Figs. 16c and d show the plots of the absolute value of the slip ratio and the velocity of the chassis, respectively, for the same terrain. As can be seen the velocity vehicle becomes negative when it encounters the discontinuity and the maximum velocity with which the vehicle traverses the terrain is less than 1 m/s. The attached video file has the MSC VisualNastran Simulation. Table 1 summarizes the simulation results and mentions the traversibility of the vehicles on each of the terrains.

5. Conclusions

In this two models of linear force actuator based active suspension vehicles have been presented and their force controllability of these vehicles has been depicted using feasibility plots, which is a unique contribution of this work. The terrain traversability of these vehicles has been shown through simulations. The proposed design based on linear force actuator allows for active control of normal forces and hence the no-slip margin at the wheel–ground contact points. Passive suspensions redistribute normal forces by changing the posture without the help of any actuators. Redistribution merely allows for increasing the normal forces at some wheels at the expense of the others or a posture can be attained where the normal force distribution at all the wheels are same. But in case of LFA-V the normal forces can be independently controlled and even create a situation where the summation of all the normal forces at the wheel–ground contact point is greater than the weight of the system. Moreover, it has also been shown that it is possible to control the posture of the vehicle while doing force control and hence the vehicle has the ability to avoid unstable configurations. The most complex of the proposed design is the LFAV-2, which utilizes 2 actuators per leg to control the internal configuration. Similar competing mechanisms such as HYLOS [8] also use same number of actuators. Hence, there is not much increase in the complexity in terms of actuator requirement when compared to the existing mechanisms.

Appendix A. Supplementary Materials

Supplementary data associated with this article can be found in the online version at doi:10.1016/j.actaastro.2010.06.051.

References

[1] T. Estier, Y. Crausaz, B. Merminod, M. Lauria, R. Piguet, R. Siegwart, An innovative space rover with extended climbing abilities, in: Proceedings of the International Conference on Robotics in Challenging Environments, Albuquerque, USA, 2000.
[2] R. Volpe, J. Balaram, T. Ohm, R. Ivlev, Rocky 7: a next generation mars rover prototype, J. Adv. Robotics 11 (4) (1997) 341–358.
[3] K. Iagnemma, A. Rzepniewski, S. Dubowsky, P. Schenker, Control of robotic vehicles with actively articulated suspensions in rough terrain, Autonomous Robots 14 (1) (2003) 5–16.
[4] S.V. Sreenivasan, K.J. Waldron, Displacement analysis of an actively articulated wheeled vehicule configuration with extensions to motion planning on uneven terrain, ASME J. Mech. Des. 118 (6) (1996) 312–317.
[5] Ch. Grand, F. BenAmar, F. Plumet, Ph. Bidaud, Stability and traction optimization of a reconfigurable wheel-legged robot, Int. J. Robotics Res. (2004).
[6] K. Iagnemma, S. Dubowsky, Traction control of wheeled robotic vehicles in rough terrain with application to planetary rovers, Int. J. Robotics Res. 23 (10–11) (2004) 1029–1040.
[7] John J. Craig, Introduction to Robotics—Mechanics and Control, Third ed., Prentice Hall.
[8] Ch. Grand, F. BenAmar, F. Plumet, Ph. Bidaud, Decoupled control of posture and trajectory of the hybrid wheel-legged robot hylos, in: Proceedings of the IEEE International Conference on Robotics and Automation, vol. 5, New Orleans, LA, 2004, pp. 5111–5116.
[10] Siddharth Sanan, Nageshwara Rao, K. Madhava Krishna, Sartaj Singh, On improving the mobility of vehicles on uneven terrain, Proceedings of ICAR-2007.
[11] 〈http://ieeexplore.ieee.org/iel5/6/30812/01426959.pdf?isnumb〉.
[12] 〈http://www.moticont.com/voice-coil-motor.htm〉.
[13] N. Chakraborty, Ashitava Ghosal, Dynamic modeling and simulation of a wheeled mobile robot for traversing uneven terrain without slip, Trans. ASME J. Mech. Des. 127 (2005) 901–909.
[14] M. Lauria, Y. Piguet, R. Siegwart, Octopus: an autonomous wheeled climbing-robot, CLAWAR (2002).
[15] Vijay P. Eathakota, Srikanth Kolachalama, K. Madhava Krishna, Siddharth Sanan, Optimal posture control for force actuator based articulated suspension vehicle for rough terrain mobility, CLAWAR (2008).

Please cite this article as: V.P. Eathakota, et al., Two models of force actuator based active suspension mechanisms for mobility on uneven terrain, Acta Astronautica (2010), doi:10.1016/j.actaastro.2010.06.051